Root metaxylem area influences drought tolerance and transpiration in pearl millet in a soil texture dependent manner

Pablo Affortit[1], Awa Faye[2*], Dylan H. Jones[3*], Ezenwoko Benson[4*], Bassirou Sine[2], James Burridge[1], Mame Sokhatil Ndoye[2], Luke Barry[1], Daniel Moukouanga[1], Stephanie Barnard[3], Rahul Bhosale[3], Tony Pridmore[4], Pascal Gantet[1], Vincent Vadez[1,2], Philippe Cubry[1], Ndjido Kane[2], Malcolm Bennett[3], Jonathan A. Atkinson[3], Laurent Laplaze[1], Darren M. Wells[3], Alexandre Grondin[1,2]

[1] DIADE, IRD, Université de Montpellier, CIRAD, Montpellier France

[2] CERAAS, Institut Sénégalais des Recherches Agricoles (ISRA),Thiès, Senegal

[3] School of Biosciences, University of Nottingham, Sutton Bonington, United Kingdom

[4] School of Computer Science, University of Nottingham, United Kingdom

*These Authors contributed equally

Authors for correspondence:

Alexandre Grondin

Email: alexandre.grondin@ird.fr

Darren Wells

Email: darren.wells@nottingham.ac.uk

Word counts: 8049

Number of main figures (all in colour): 5

Number of supporting figures (all in colour): 20

Number of tables: 2

Number of supporting tables: 1

Number of supporting excel files: 1

Summary

- Pearl millet is a key cereal for food security in drylands but its yield is strongly impacted by drought. We investigated how root anatomical traits contribute to mitigating the effects of vegetative drought stress in pearl millet.
- We examined associations between root anatomical traits and agronomical performance in a pearl millet diversity panel under irrigated and vegetative drought stress treatments in field trials. The impact of associated anatomical traits on transpiration was assessed using subpanels grown in different soil within a greenhouse.
- In the field, total metaxylem area was positively correlated with grain weight and its maintenance under drought. In the greenhouse, genotypes with larger metaxylem area grown in sandy soil exhibited a consumerist water use strategy under irrigation, which shifted to a conservative strategy under drought. Water savings was mediated by transpiration restriction under high evaporative demand. This mechanism was dependent on soil hydraulics as it was not observed in peat soil with higher hydraulic conductivity upon soil drying.
- We propose that water savings under drought, mediated by large metaxylem area and its interaction with soil hydraulics, help mitigate vegetative drought stress. Our findings highlight the role of soil hydraulic properties in shaping plant hydraulics and drought tolerance.

Key words: Pearl millet, drought, metaxylem vessel, axial root hydraulic conductance, transpiration restriction, soil hydraulics.

Introduction

Pearl millet is a C4 plant with high nutritional quality that was domesticated about 4,500 years ago in the Sahel region (Burgarella *et al.*, 2018). It is the sixth most important cereal crop globally, and its production is concentrated in the arid and semi-arid regions of Western and Central Africa as well as India (Varshney *et al.*, 2017). It plays a major role for food security in these regions, serving as a subsistence crop and an important source of revenue for smallholder farmers (FAOSTAT, 2024). Although pearl millet is considered as one of the most heat and drought stress tolerant cereal crops, its production is strongly impacted by climate change (Debieu *et al.*, 2017). Pearl millet yield losses due to drought in Sahelian conditions have been estimated at up to 65% during early-stage and vegetative drought stress (i.e. before flowering), with lower losses observed during terminal drought stress (i.e. post flowering; Mahalakshmi *et al.*, 1987; Winkel *et al.*, 1997). A modelling approach using climatic data collected from 2000 to 2020 in Senegal suggested that vegetative drought stress occurred more frequently than terminal drought stress (24% of the years against 19%, respectively), resulting in a stronger impact on biomass (44% yield loss against 12%, respectively) and grain yield (43% yield loss against 25%, respectively; Fuente *et al.*, 2024). In West African traditional farming systems, vegetative drought stress affecting pearl millet often occurs because the crop is typically cultivated under rainfed conditions and sown before or immediately after the first rain, a period characterized by erratic rainfall and potential dry spells lasting several weeks. As current models predict an increase in the frequency of these dry spells in future climate (Sultan & Gaetani, 2016), improving pearl millet's tolerance to vegetative drought stress is becoming increasingly urgent.

Drought stress occurs when water availability insufficient to meet the plant's needs for optimal growth. Roots play a critical role in plant water availability and overall plant hydraulics by controlling the access and transport of water to the shoots (Vadez *et al.*, 2024). Crops could be bred for root traits that more efficiently and effectively acquire and transport soil water resources, leading to improved drought tolerance (Lynch *et al.*, 2021). However, breeding programs have often overlooked root traits in efforts to enhance drought tolerance in crops, because roots are challenging to phenotype in soils and root pre-breeding research is frequently difficult to translate into practical applications in farmer's fields (Ndoye *et al.*, 2022). While technologies for high-throughput phenotyping of roots are advancing (Atkinson *et al.*, 2019; Li *et al.*, 2022), current research emphasizes field phenotyping of roots (Lynch *et al.*, 2021) and aims to better comprehend the complex interplay between root and soil properties on whole

plant water uptake (Cai *et al.*, 2022). Recent data suggest that as soil dries, stomatal closure is influenced by plant traits related to root hydraulic conductance, as well as by soil texture (Carminati & Javaux, 2020; Cai *et al.*, 2022). For instance, maize plants with larger root and rhizosphere systems were able to delay the impacts of soil hydraulic limitations on transpiration in drying soils (Koehler *et al.*, 2023), a phenomenon influenced by soil texture (Koehler *et al.*, 2022). The ability of pearl millet to thrive in marginal soils with low water retention, while enduring high levels of drought stress, suggests that this species possesses root hydraulic mechanisms that effectively regulate water flow across the soil-plant-atmosphere continuum.

Architectural root traits play a crucial role in determining a plant's capacity to access water. Deeper root growth is one such trait that helps mitigate the effects of drought stress (Uga *et al.*, 2013; Bacher *et al.*, 2023). Early pearl millet root growth is characterised by a single primary root being the only architectural component for the first six days (Passot *et al.*, 2016). The fast growth of this primary root at depth was associated with improved tolerance to post-germination drought stress under field conditions (Fuente *et al.*, 2024). Additional work suggested that, during later stages of pearl millet root development, larger root surface active for water uptake limited the drop in soil water potential around the root and allowed maintenance of transpiration in drying soils (Cai *et al.*, 2020). In addition to these architectural traits, root anatomical differences significantly affect plant's capacity to acquire water under drought stress (Lynch *et al.*, 2014; Vadez *et al.*, 2024). For example, a reduction in xylem diameter has been shown to improve drought tolerance in wheat by slowing root water uptake and overall plant water use (Richards & Passioura, 1989). Other traits such as root diameter, the presence of cortical aerenchyma, and a reduced number of cortical cell layers, enhance water uptake efficiency by lowering the metabolic cost of root growth (Zhu *et al.*, 2010; Chimungu *et al.*, 2014a; Sidhu & Lynch, 2024). Moreover, suberization of the endodermis or exodermis layers influences radial water transport (Henry *et al.*, 2012; Cantó-Pastor *et al.*, 2024). However, little is known about the pearl millet root anatomy, its diversity, and its impacts on root water uptake in relation with soil texture in the context of drought.

In this study, we investigated root anatomical traits in a diverse panel of pearl millet genotypes grown in the field under both irrigated and vegetative drought stress treatments over two consecutive years. We also analysed the variation in shoot biomass and grain weight responses to vegetative drought stress, and linked these to root anatomical traits to determine if any of the later traits were associated with improved drought tolerance. A correlation between total

metaxylem area and grain weight and grain weight maintenance under drought was observed. The influence of this trait on transpiration dynamics was further assessed using contrasting subpanels grown in different soil types on a lysimetric platform installed within a greenhouse.

Material and Methods

Plant material

One hundred sixty two pearl millet genotypes selected from the pearl millet genetic association panel (PMiGAP; Sehgal *et al.*, 2015) were used in this study (Supplementary file **S1**). This panel of inbred lines is composed of cultivated germplasm originating from Africa and India and elite improved open-pollinated cultivars, and is representative of the genetic diversity of pearl millet (Sehgal *et al.*, 2015; Varshney *et al.*, 2017). We included in this panel Tift23DB that has been used to produce the pearl millet reference genome sequence (Varshney *et al.*, 2017; Salson *et al.*, 2023), four inbred mapping population parents (ICML-IS11084 and ICML-IS11139 contrasting for soil aggregation, and ICML-IS11155 and SL2 contrasting for primary root length; Fuente *et al.*, 2022; Fuente *et al.*, 2024) and five inbred lines from West Africa (Debieu *et al.*, 2018) and four Senegalese breeding lines. Seeds from the same multiplication were used in both field trials to ensure the genetic uniformity of the genotypes and avoid seed lot effects.

Field experiments

Pearl millet genotypes were grown in a soil of loamy sand texture (84.8% sand, 7.9% silt and 7.2% clay with a bulk density of 1.7 g cm^{-3} in average from 0 to 200 cm depth; Diongue *et al.*, 2022) under irrigated and drought stress treatments over two years (2021 and 2022) in the CNRA research station in Bambey, Senegal (14°42'48.3"N 16°28'41.2"W). The field was laid out using an Alpha Lattice design for each treatment, each including one hundred sixty genotypes with four repetitions or complete blocks that were composed of 10 subblocks. Fifteen genotypes differed from 2021 to 2022 (Supplementary file **S1**). Each subblock included 16 plots and each plot contained 24 hills of one plant of the same genotype (3 rows of eight plants with 90 cm distance between rows and 30 cm distance between plants within the row; Fig. **S1**). Plants were sown in the dry season (early March in 2021 and late March in 2022) to fully control the water supply (weather data are presented in Table **S1**). After sowing, plants were irrigated with 30 mm of water twice a week before application of the drought stress treatment. Drought stress was imposed by withholding water from 21 to 49 days after sowing (DAS) in 2021 and from 21 to 42 DAS in 2022. Both treatments were then irrigated with 30

mm of water twice a week until maturity. Volumetric soil water content was monitored between 0 and 160 cm depth using DIVINER probes (Sentek Pty Ltd) installed throughout the field (Fig. **S2**).

At the end of the drought stress treatment, three representative plants per plot were harvested for crown root anatomical phenotyping following the shovelomics method developed by Trachsel *et al.* (2011) and shoot biomass (SDW) measurement. Crown roots from node four were collected (2 cm segment located approximately 1 cm away from the shoot base) and immediately stored in 50% (v/v) ethanol in water. Roots from this node were chosen because they emerged around 21 DAS, which corresponds to the time of drought stress imposition (Ndoye *et al.*, 2024). Furthermore, they were easier to identify and sustained less damage than roots from earlier nodes during sampling.

Phenology, shoot morphology and biomass at maturity, as well as grain weight and yield component traits were measured on three plants per plot as in Debieu *et al.* (2018). The stress tolerance index (STI) defined in Fernandez (1992) was used to evaluate shoot biomass and grain weight (GW) maintenance under drought stress in the panel. This index was calculated on several variables (Var) as :

$STI_{Vari}=(Var_{wi}* Var_{Di})/(Var_w)^2$

where Var_{wi} is the variable value measured under irrigated condition for genotype *i*, Var_{Di} is the variable value measured under drought stress treatment for genotype *i*, Var_w is the variable mean value under irrigated condition for all tested genotypes. The STI was measured on grain weight (STI GW), on shoot biomass after the drought stress treatment (STI SDW 49 DAS in 2021 and STI SDW 42 DAS in 2022) and at maturity (STI SDW Mat). STI is a useful metric to compare individual genotypes tolerance to drought while considering its performance under irrigated treatment.

Crown root anatomical phenotyping

Root anatomical phenotyping was performed using laser ablation tomography (LAT) at the Sutton Bonington campus of the University of Nottingham (UK). Root samples in 50% (v/v) ethanol solution were transferred to custom holders (each holding 48 roots) and moved to a 70% (v/v) ethanol solution for 48 h. Filled holders were then transferred to 100% methanol for a further 48 h before a final transfer to 100% ethanol for a minimum of 48 h prior to critical point drying. Three holders were then transferred to a critical point dryer (Model EM CPD300,

Leica Microsystems) and dried by exchange with liquid carbon dioxide. Once dried, holders were stored in containers with silica gel as a desiccant.

LAT uses an ultrafast UV laser to ablate sections from a root sample prior to imaging of the exposed surface, which is illuminated and caused to autofluoresce by the UV laser. Progressing the sample into the ablation plane allows serial imaging of exposed internal surfaces (Chimungu *et al.*, 2015; Hall *et al.*, 2019; Strock *et al.*, 2019; Cunha Neto *et al.*, 2023). The tomograph used in this study (LATScan, Lasers for Innovative Solutions LLC) uses a Q-switched UV (355 nm) picosecond-pulsed laser source (Model PX100-3-GF, EdgeWave GmbH) outputting into a galvanometer (Model RTC4, Scanlab GmbH) that focuses the beam via a 160 mm f-theta objective lens. Beam parameters are set by the SPiiPlus software (ACS Motion Control) that also controls a nanopositioning z-stage (PIMag, Physik Instrumente) to advance the sample into the ablation plane. Samples are held in custom holders mounted on XY linear actuators for positioning. Imaging is via a custom system that uses infinity-corrected long working distance objectives (1X – 20X) mounted on a video microscope unit fitted with an objective turret (Model WIDE VMU-H, Mitutoyo (UK) Ltd.) and a 12.3 MP machine vision camera (Model Grasshopper3, FLIR). A third linear actuator, also on the Z plane, positions the imaging system for fine adjustment of focus. An interface written in the LabVIEW development platform (National Instruments Corp.) allows user control of the focus and positioning actuators, camera settings and real-time monitoring of ablation.

An automated sketch in SPiiPlus was used to capture a series of images from critically point dried samples. A series of 10 ablations was performed, first to cut the root at the focal point of the objective, then to 'polish' the newly exposed surface by removing any artefacts resulting from thermal ablation, followed by 5 ablations combined with imaging at a z-step size of 10 µm. The sample was then progressed 500 µm into the beam path and the process repeated three times to give a total of 20 images across a 2.6 mm length of root. From the set of 20 imaged sections from each root sample, a representative image was curated for subsequent quantification. These were initially selected from the middle of the image stack, then resampled as necessary to replace images containing features that would hinder analysis, such as points of lateral root emergence, signs of mechanical damage, or uneven laser illumination.

Annotated root images were produced using the CellSeT software tool (Pound *et al.*, 2012) to produce a training set for a convolutional neural network for segmentation and quantification based on RootScan and RootScan2 software (Burton *et al.*, 2012;

https://plantscience.psu.edu/research/labs/roots/methods/computer/rootscan). Nine tissue types consisting of epidermis, sclerenchyma (SCL), cortical cell, aerenchyma, endodermis, stele cell, metaxylem vessels (MX) and vascular bundles were tagged (Fig. **S3**), and an initial set of 200 annotated pearl millet images augmented by rotation, contrast enhancement and degradation, addition of noise, and reflection were used to increase the size of the training set to a total of 1200 images (200 annotated image and 1000 augmented images). The network was created using the PyTorch machine learning framework using a combination of Python and C^{++}. Unsupervised training and model generation was run on the University of Nottingham Augusta High Performance Cluster. The training set was supplemented ad hoc by an additional 20 annotated images to improve inaccuracies associated with particular image qualities. The output of the model is a segmented annotated cell mask from which measurements were generated. Features were measured by a combination of pixel and feature counting, and the fitting of circles and convex hulls to the segmentation mask (Fig. **S3b**).

Crown root anatomical phenotyping along node four in rhizotrons

Root anatomy along the length of crown roots from node four were measured on four genotypes selected for their contrast in total metaxylem area: IP-14210 and IP-5031 are genotypes with small metaxylem area and IP-7536 and IP-6098 are genotypes with large metaxylem area. Seeds were sown in rhizotrons (soil volume -1000 mm x 700 mm x 45 mm) filled with a sandy loam soil (72% sand, 15% silt, 13% clay) irrigated at field capacity in a greenhouse facility at the Sutton Bonington campus of the University of Nottingham (UK) in the 2023 summer season (July-August). Six plants per genotype were planted with one plant per rhizotron for a total of 24 rhizotrons that were randomised in the greenhouse. Temperature was set at 30°C during the day and 24°C at night with 12 hours of artificial lightning from 7AM to 7PM. Plants were well irrigated until harvest at 28 DAS. One whole crown root was then collected on node 4 for each plant and placed in 50% (v/v) ethanol in water. Root samples were collected for LAT imaging at three positions along the root length: at 1 cm from the base of the stem (Base) as in the field experiment, at the middle of the root (Middle) and at 5 cm from the root tip (Apex).

Transpiration measurements in the greenhouse

Greenhouse experiments were conducted in spring 2023 and 2024 (March-April) at IRD Montpellier (France). In 2023, twelve genotypes contrasted for total metaxylem area but showing no significant differences in terms of shoot biomass measured at 49/42 DAS under irrigated conditions in the field experiments (IP-10539, IP-11929, IP-12395, IP-14210, IP-

17150, IP-18168, IP-19626, IP-22494, IP-5031, IP-6098, IP-7536, IP-9496) were cultivated under irrigated and drought stress treatments in an organic potting substrate (referred hereafter as peat soil) in 5.5-liter pots (19 cm top diameter, 15.5 cm bottom diameter and 25 cm depth). The potting substrate (GO M2 140 substrate, Jiffy Group) was composed of crushed baltic white peat (75%), coconut peat (20%) and sand (5%). It was implemented with optimal fertilisation for pearl millet growth. Pots were placed on load cells (240 in total) installed within the greenhouse. The load cells were set to monitor pot weight every 30 min (Phenospex Ltd). The temperature in the greenhouses was set at 28°C during the day and 25°C at night. Daylength was controlled by artificial lighting (900 W m^{-2}) from 7AM to 7PM. Relative humidity, temperature and solar radiation were monitored in the greenhouse. Genotypes were completely randomised with six replicates per treatment. In each replication, both treatments were positioned side by side in the greenhouse to limit positioning effects. In 2024, twenty genotypes contrasting for the same criteria (IP-11929, IP-12395, IP-14210, IP-17150, IP-18168, IP-19626, IP-22494, IP-5031, IP-6098, IP-7536, IP-9496 from the 2023 experiment implemented with IP-10759, IP-10964, IP-12364, IP-15533, IP-17611, IP-21206, IP-22420, IP-22423, IP-5272) were grown in similar conditions except that the soil used was a mix at equivalent volume (50:50 v/v) of the previous potting substrate with fine sand (AF0/1RS, DIALL) of particle size below 1 mm (referred hereafter as sandy soil).

Plants were well irrigated until 20 DAS. At this date, pots were saturated and drained overnight. At 21 DAS, a layer of plastic beads was added on the soil surface in order to prevent soil evaporation and pots weight were measured to record the weight at field capacity. An experiment performed beforehand following a similar set up was conducted for each soil to determine the coefficient of pot weight reduction from field capacity to soil water content at which the plant stopped transpiring. These coefficients (70% and 30% reduction of the initial pot weight for the peat soil and for the sandy soil, respectively) were used to approximate, from the pots saturated weights, the pots weight at which plant transpiration theoretically stopped. The difference between the weight at field capacity and the weight at which transpiration stopped corresponded to the fraction of transpirable soil water (FTSW). FTSW was further used to monitor soil water content through daily recordings of pots weight at 3PM. The drought stress treatment of the peat soil experiment consisted in a dry down to FTSW 40% (pot weight when 40% of the water usable for transpiration is left) that was maintained till harvest (42 DAS). The drought stress treatment of the sandy soil experiment consisted in a progressive dry-down so all plants reached FTSW 75% (at 28 DAS), then FTSW 60% (at 35 DAS) and

289 FTSW 40% (at 40 DAS), after which irrigation was stopped until harvest (42 DAS). In the
290 irrigated treatment of both experiments, soil moisture was maintained at FTSW 75% until
291 harvest.
292
293 At harvest, leaves were collected to measure leaf area using a planimeter (LI-3100C, LI-COR).
294 Leaves and stems were further oven dried for three days at 70°C to measure dry biomass. For
295 each plant, crown roots from nodes one to five in the peat soil experiment and from nodes three
296 and four in the sandy soil experiment were collected and stored in 2 ml tubes filled with 50%
297 (v/v) ethanol in water for LAT. Root theoretical axial hydraulic conductance (K_x in $m^4\ s^{-1}$
298 MPa^{-1}) was estimated as the sum of the theoretical axial root hydraulic conductance of each
299 individual metaxylem vessels present in the root cross section using the following modified
300 Hagen-Poiseuille equation:

$$K_x = \sum_{i=1}^{N} \frac{\pi d_i^4}{128\eta}$$

301
302 where N is the number of xylem vessels in a root cross section, d is the diameter of one
303 individual xylem vessel in the root cross section and η is the viscosity of water
304 (1.0021×10^{-9} MPa s^{-1} at 20°C; Nobel, 2009).
305
306 Slopes of the transpiration response to the evaporative demand were calculated at 41 DAS in
307 both greenhouse experiments using an automated pipeline described by Kar *et al.* (2020).
308 Briefly, plant transpiration (Tr) was first calculated as the difference in pot weights within
309 intervals of 30 minutes. Transpiration rate (Tr Rate) was further measured by dividing Tr by
310 the time interval and plant leaf area, assuming marginal changes in leaf area between 41 and
311 42 DAS. At each time interval, reference evapotranspiration (ETref) was calculated according
312 to the Penman-Monteith equation using actual climatic data within the greenhouse (Zotarelli *et*
313 *al.*, 2010). Slopes of transpiration response to the evaporative demand (Slope Tr) were
314 calculated from 7AM to 3:30PM (which corresponded to the maximum evaporative demand of
315 the day) by plotting the Tr Rate against the ETref. Profiles of Tr along the day were plotted for
316 two groups of genotypes contrasting for their theoretical axial root hydraulic conductance (K_x).
317
318 **Data analysis**

Outliers within each genotype were statistically removed using the interquartile method in R for all measured traits in each experiment (ggplot2 v0.6.0 boxplot. stats et grDevices v4.3.3). Data obtained from each field experiment were further corrected for spatial heterogeneity by treatments using the Spatial Analysis of Trials using splines (SpATs) function in the StatgenSTA package in R (Rodríguez-Álvarez *et al.*, 2018; van Rossum, 2024), considering a resolvable incomplete block design model. In this model, genotype was fitted as a fixed effect and Best Linear Unbiased Estimates (BLUEs) were produced. Heritability, considered as the ratio of genetic variance to phenotypic variance, was calculated in StatgenSTA for each trait using a similar model but fitting the genotype as a random effect. To correct for spatial heterogeneity in the greenhouse experiments, a similar approach was followed but using the SpATS model in the StatgenHTP package in R (Millet *et al.*, 2021) which allows spatial correction on individual plants.

Statistical analysis

Statistical analyses were carried out in R (V 4.3.3; R Development Core Team, 2008). Normality of the different traits were verified using the Shapiro-Wilk test and the equality of variances using the Levene test. Trait means between treatments within years were compared using the Wilcoxon test. The Student t-test was used to compare mean values of total metaxylem area in the rhizotron experiment and transpiration (Tr) in the greenhouse experiments. Correlations between variables were investigated using the Pearson correlation test using BLUEs.

Results

Vegetative drought stress negatively impacts shoot biomass production and grain weight in pearl millet

Field trials were conducted over for two consecutive years (2021 and 2022) at CNRA Bambey in Senegal, using diverse pearl millet genotypes. Genotypes were cultivated either under irrigated treatment or subjected to vegetative drought stress by withholding irrigation 21 days after sowing. The drought stress lasted four weeks (from 21 to 49 DAS) in 2021 and three weeks (from 21 and 42 DAS) in 2022. After the stress period, crown roots from node four were sampled for anatomical phenotyping and shoot biomass was measured. Irrigation was then resumed until maturity, at which agro-morphological and yield component traits were measured to study the diversity of drought responses within the panel.

A large variability in all agronomic traits was observed, under both irrigated and drought stress treatments (Table **1**). Heritability ranged from 0.4 for shoot biomass measured at 49 DAS under drought in 2021 to 0.9 for days to flowering in both years and treatments, indicating that these traits are under strong genetic control (Table **1**). Furthermore, positive and significant correlations were observed for both agro-morphological and yield component traits between the two years under irrigated and drought treatments (Fig. **S4**), illustrating the robustness of the measured traits from one year to the next.

Drought stress significantly reduced shoot biomass measured at 49 and 42 DAS in both years, with a 60% and 61% average reduction in 2021 and 2022, respectively (Fig. **1a**). At maturity, partial recovery in shoot biomass was observed with average reduction of 46% in 2021 and 25% in 2022 (Fig. **1b**). However, grain weight was reduced by 53% in 2021 and 37% in 2022 (Fig. **1c**). The drought stress also had a negative and significant impact on plant height, the number of tillers, and thousand grain weight in both years (Fig. **S5**).

The stress tolerance index (STI) was used to measure maintenance of shoot biomass at the end of the drought stress period, as well as the maintenance of shoot biomass and grain weight at maturity. This index corresponds to an indicator of drought tolerance and performance under irrigated conditions, both of which are crucial for breeding purposes. Large variation in stress tolerance index for both shoot biomass measured at the end of the drought stress and at maturity, and for grain weight, was observed in each year, with values significantly correlated between years (R = 0.51 for grain weight; Fig. **1d** and **S6**). The stress tolerance index for grain weight varied from low values (0.02 at lowest in 2021 and 2022) for genotypes performing poorly under both irrigated and drought stress treatments to values above 1 (1.3 at highest in 2021 and 1.8 in 2022) for genotypes performing well under both treatments. Furthermore, the stress tolerance index for grain weight was positively correlated with the stress tolerance index for shoot biomass measured at the end of the drought stress and at maturity in both years (Fig. **1e**,**f**), suggesting that maintaining shoot biomass production under stress was associated with grain weight maintenance.

Altogether, the field trials revealed a large phenotypic diversity for shoot morphological and agronomical traits in pearl millet. Vegetative drought stress had a significant impact on most traits, with genotypes better able to maintain shoot biomass production during the stress period showing improved grain weight maintenance under drought.

Table 1 Variation for morphological and agronomical traits in the field trials.

Mean: Mean of n = 4. SD: Standard deviation; CV: Coefficient of variation; H^2: Heritability.

Acronym	Trait	Year	Treatment	Mean	SD	CV	H^2
GW	Grain weight (g plant^{-1})	2021	WW	89	39	1488	0.5
			WS	43	26	694	0.6
		2022	WW	71	36	1262	0.7
			WS	46	28	810	0.6
DTF	Days to 50% flowering	2021	WW	58	7.5	56	0.9
			WS	65	9.2	83	0.9
		2022	WW	64	11	115	0.9
			WS	71	13	182	0.9
SDW	Shoot biomass at the end of the stress (g plant^{-1})	2021	WW	55	28	769	0.6
			WS	20	12	154	0.4
		2022	WW	27	15	221	0.7
			WS	10	5.8	34	0.6
SDW Mat	Shoot biomass at maturity (g plant^{-1})	2021	WW	169	71	5017	0.7
			WS	87	52	2717	0.7
		2022	WW	196	93	8675	0.8
			WS	151	78	6080	0.8
1000-grain weight	1000 grains weight (g plant^{-1})	2021	WW	8.5	1.6	2.66	0.6
			WS	7.4	1.7	2.8	0.8
		2022	WW	8.6	2.2	4.8	0.8
			WS	8.3	1.9	3.57	0.8
Tiller number	Number of tillers	2021	WW	9.8	4	15.65	0.5
			WS	8.3	3.9	15.19	0.7
		2022	WW	9.9	3.4	11.3	0.7
			WS	8.7	2.7	7.41	0.7
Plant height	Plant height at maturity (cm)	2021	WW	155	29	856	0.9
			WS	122	31	956	0.8
		2022	WW	144	28	776	0.9
			WS	131	34	1131	0.9

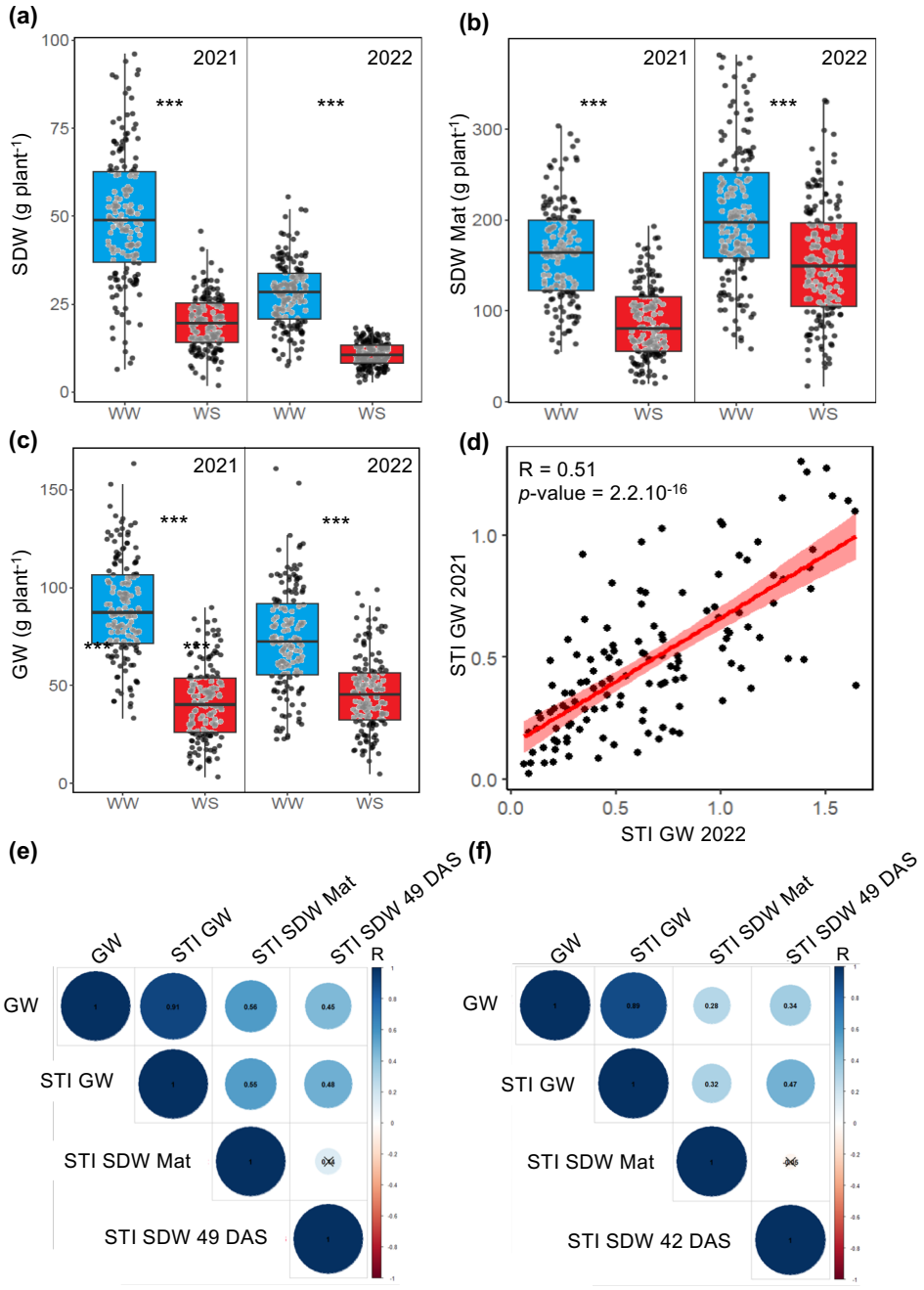

Fig. 1 Drought stress effects on shoot biomass and grain yield in the field. (a) Shoot biomass at the end of the drought stress (SDW 49 DAS in 2021 and SDW 42 DAS in 2022), (b) shoot biomass at maturity (SDW Mat), and (c) grain yield (GW) were measured in the field on diverse pearl millet genotypes under well-watered (WW) and drought stress (WS) treatments in 2021 and 2022. *** p-value < 0.001 according to a Wilcoxon test. (d) Covariation between stress tolerance index for grain yield (STI GW) measured in 2021 and 2022. The Pearson correlation coefficient (R) and p-value of the correlation test are indicated. (e, f) Correlation between grain weight (GW), the stress tolerance index for shoot biomass measured at the end of the drought stress (STI SDW 49 DAS in 2021 and STI SDW 42 DAS in 2022), the shoot biomass measured

at maturity (STI SDW Mat) and the stress tolerance index for grain yield (STI GW) in 2021 (e) and 2022 (f). Boxplots and correlation analyses were performed using the best linear unbiased estimates. The Pearson correlation coefficient (R) is indicated for each pair of traits and black crosses indicate non-significant correlation (p-value > 0.05).

Metaxylem area positively associates with grain weight production and maintenance under early drought stress

To identify root anatomical traits that contribute to grain weight and its maintenance under vegetative drought stress in pearl millet, cross-sectional images of crown roots sampled from node four at the end of the drought stress in the field were obtained using laser ablation tomography (LAT) and anatomical traits were measured using an updated version of RootScan for pearl millet (Fig. **2a,b,c**). Traits of the epidermis, cortical cells, aerenchyma, endodermis and vascular bundle were excluded due to lower measurement reliability.

Large variation in for total metaxylem area, number of metaxylem vessels, mean area of individual metaxylem vessels, root cross section area, stele area, sclerenchyma area, ratio between stele area and root cross section area, and the ratio between sclerenchyma area and root cross section area were observed within the panel under both treatments (Table **2**). The heritability of these traits varied from 0.4 for total metaxylem area measured in the 2021 drought stress treatment to 0.81 for mean area of individual metaxylem vessels measured in the 2022 irrigated treatment (Table **2**). Positive and significant correlations were observed for root anatomical traits between years under irrigated treatment (Fig. **S7**). Under drought stress, a similar trend was observed, but, correlations between years were weaker and only significant for root cross section area, stele area and metaxylem-related traits (Fig. **S7**). Within years, drought stress significantly negatively impacted all measured root anatomical traits in 2021, but only affected stele area and the ratio between stele area and root cross section area in 2022 (Fig. **S8**).

We further investigated correlations between root anatomical traits, shoot biomass, grain weight and the stress tolerance indices. Positive and significant correlations were observed in both years between total metaxylem area and grain weight measured under drought stress, and stress tolerance index for grain weight (Fig. **2d**). Similar correlations were observed between mean area of individual metaxylem vessels and grain weight measured under drought stress, and stress tolerance index for grain weight (Fig. **2d**). These metaxylem traits measured under

irrigated treatment were also correlated with grain weight measured in the same condition and the stress tolerance index for grain weight in both years (Fig. **S9**). This suggests that pearl millet genotypes with larger total metaxylem area were both more productive under irrigated treatment and more tolerant in terms of grain weight under vegetative drought stress. Positive and significant correlations were also observed between the stele area and the ratio between stele area and root cross section area measured under drought stress and the stress tolerance index for grain weight, although only significant in 2022 (Fig. **2d**). Similarly, negative and significant correlations between the ratio of sclerenchyma area and root cross section area measured under drought stress and stress tolerance index for grain weight were observed only in 2022 (Fig. **2d**).

Hence, several root anatomical traits were associated with grain weight under both irrigated and drought stress treatments in pearl millet. Among them, total metaxylem area and mean area of metaxylem vessels were the most consistently positively associated with grain weight under both treatments and its maintenance under drought.

Table 2 Variation for root anatomical traits in the field trials.

Mean: Mean of n = 4. SD: Standard deviation; CV: Coefficient of variation; H^2: Heritability

Acronym	Trait	Year	Treatment	Mean	SD	CV	H^2
Total MX area	Total cross section area of metaxylem vessels (µm²)	2021	WW	62092	23958	5.7E+08	0.7
			WS	54159	22302	5E+08	0.4
		2022	WW	54516	19448	3.8E+08	0.75
			WS	53051	18899	3.6E+08	0.7
Number MX	Number of metaxylem vessels	2021	WW	8.8	2.37	5.61	0.6
			WS	8.09	2.17	4.72	0.5
		2022	WW	8.33	2.09	4.35	0.63
			WS	8.15	1.95	3.81	0.6
Mean MX area	Mean area of individual metaxylem vessel (µm²)	2021	WW	6997	1899	3605854	0.8
			WS	6609	1876	3520545	0.6
		2022	WW	6535	1671	2792446	0.81
			WS	6507	1704	2904023	0.8
Root area	Total area of the root cross section (µm²)	2021	WW	2E+06	6E+05	3.26E+11	0.5
			WS	1E+06	618051	3.82E+11	0.5
		2022	WW	1238601	470466	2.21E+11	0.62
			WS	1281454	434554	1.89E+11	0.5
Stele area	Total area of the stele (µm²)	2021	WW	4E+05	2E+05	3.1E+10	0.6
			WS	4E+05	156932	2.5E+10	0.5
		2022	WW	368631	137485	1.9E+10	0.68
			WS	341123	122991	1.5E+10	0.6
SCL area		2021	WW	85108	26643	7.1E+08	0.7

	Sclerenchyma area (µm²)	2022	WS	75589	22458	5E+08	0.5
			WW	73029	22580	5.1E+08	0.53
			WS	67920	19372	3.8E+08	0.5
SR ratio	Ratio between stele area and root area	2021	WW	0.3	0.057	0.0032	-
			WS	0.273	0.061	0.0038	-
		2022	WW	0.33	0.08	0.0062	-
			WS	0.296	0.075	0.0056	-
SCL ratio	Ratio between SCL area and root area	2021	WW	0.1	0.01	0.0001	-
			WS	0.052	0.0116	0.0001	-
		2022	WW	0.06	0.01	0.0002	-
			WS	0.054	0.0115	0.0001	-

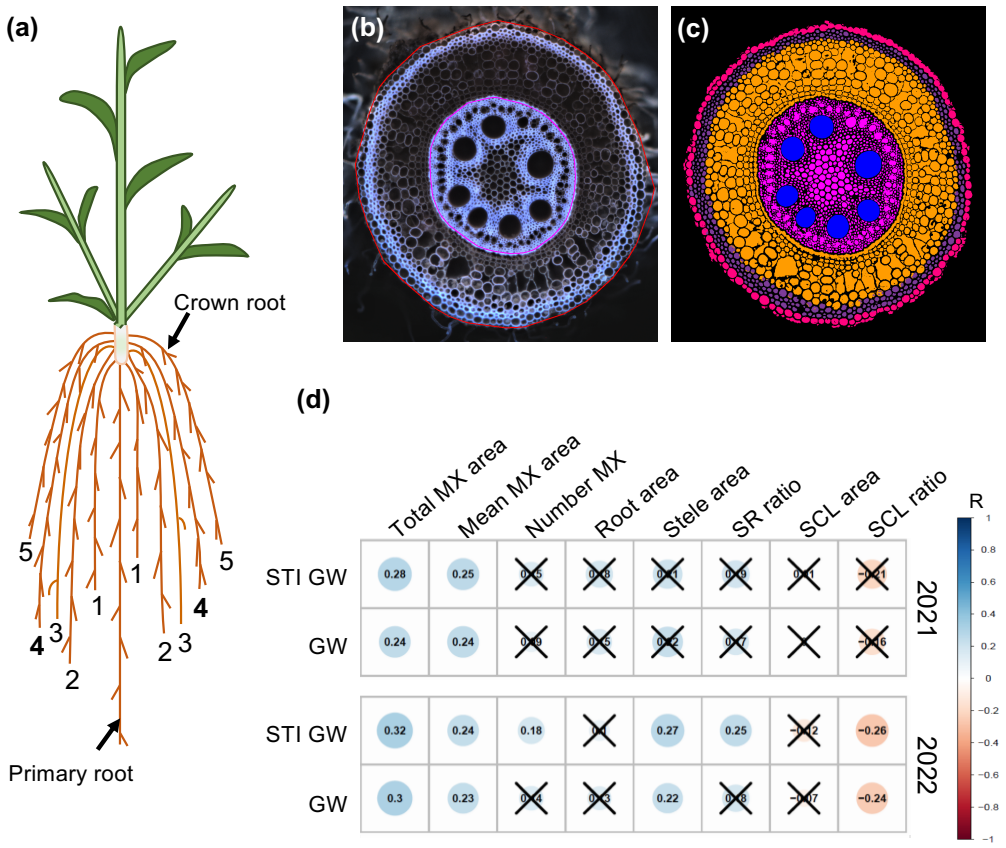

Fig. 2 Correlation between root anatomical traits and yield. (a) Schematic representation of a pearl millet root system with crown roots from different nodes. (b) Image of a pearl millet root cross section obtained through laser ablation tomography. Root cross section area (Root area; red line) and stele area (Stele area; pink line) were estimated using the convex hull approach. (c) Same image as in (b) segmented using RootScan adapted for pearl millet. Metaxylem (MX) were segmented in blue pixel and resulted in the quantification of total metaxylem area (sum of the blue pixels), number of metaxylem (number of blue objects) and mean area of one metaxylem vessel (total metaxylem area divided by the number of

463 metaxylem). Stele was segmented in pink. Cortex was segmented in orange. Sclerenchyma
464 (SCL) area was quantified as the sum of the purple pixels. Epidermis was segmented in reddish
465 purple. (d) Correlation between grain weight (GW) measured under drought stress, the stress
466 tolerance index for grain weight (STI GW) and root anatomical traits measured under drought
467 stress in the 2021 and 2022 field experiments. Correlation test was performed using the best
468 linear unbiased estimates. The Pearson correlation coefficient (R) is indicated for each pair of
469 traits and black crosses indicate non-significant correlation (p-value > 0.05). SCL ratio: ratio
470 of sclerenchyma area to root cross section area; SR ratio: ratio of stele area to root cross section
471 area.
472
473 **Metaxylem area measured on crown roots from node four are representative of the**
474 **overall plant' root metaxylem characteristics**
475 In the field trials, root anatomy was studied on crown roots from node four sampled near the
476 stem base. To determine whether metaxylem characteristics were conserved along the crown
477 root from node four, we measured root anatomy at three different locations in four genotypes
478 contrasting for total metaxylem area grown in rhizotron (Fig. **3a**). The contrast for total
479 metaxylem area observed in the field between genotypes at the stem base was conserved, with
480 IP-14210 having the smaller total metaxylem area and IP-6098 having the larger total
481 metaxylem area (Fig. **3b**). Total metaxylem area measured at the base of the stem where
482 metaxylem vessels are fully elongated, was not significantly different from that measured at
483 the middle of the root, except in IP-14210 (Fig. **3b**). However, total metaxylem area at these
484 two locations was significantly greater than that measured at the root apex, with the exception
485 of IP-14210. In fact, no contrast between genotypes was observed for total metaxylem area at
486 the root apex. The number of metaxylem vessels also correlated strongly from the stem base to
487 the root apex (Fig. **S10a**). These results suggest that variations between metaxylem-related
488 traits between pearl millet genotypes appear in the elongated root region and that variations in
489 these traits are likely similar along the root.
490
491 We next tested whether total metaxylem area measured on crown root from node four was
492 representative of total metaxylem area from roots of earlier and later nodes in 12 genotypes,
493 which differed in their total metaxylem area. These genotypes were grown in pots filled with
494 peat soil in a greenhouse. We aimed to assess total metaxylem area in crown roots from nodes
495 one and two, but, these roots were very thin, and anatomical measurements using LAT were
496 challenging. Total metaxylem area was therefore measured in roots from nodes three, four, and

five. Total metaxylem area and the number of metaxylem vessels from all nodes were positively and significantly correlated (Fig. **3c** and Fig. **S10b**), except for the number between node three and node five. The strongest correlations were observed between total metaxylem area of crown roots from adjacent nodes (nodes four and five), while the weakest correlations were observed between total metaxylem area of crown roots from nodes further apart (nodes three and five; Fig. **3c**). Total metaxylem area of crown roots increased from node three to five, but the ranking of genotypes was generally conserved from one node to another, indicating the variation in total area of metaxylem of crown roots is proportional across nodes within genotypes (Fig. **3d**).

Altogether, these results suggest that total metaxylem area measured in crown roots at the base of the stem on node four is representative of the overall root metaxylem characteristics of the plant. A plant with a smaller total metaxylem area in crown roots at the stem base of node four will likely show a smaller total metaxylem area along the crown root in the fully elongated zone and across crown roots from different nodes, and vice versa.

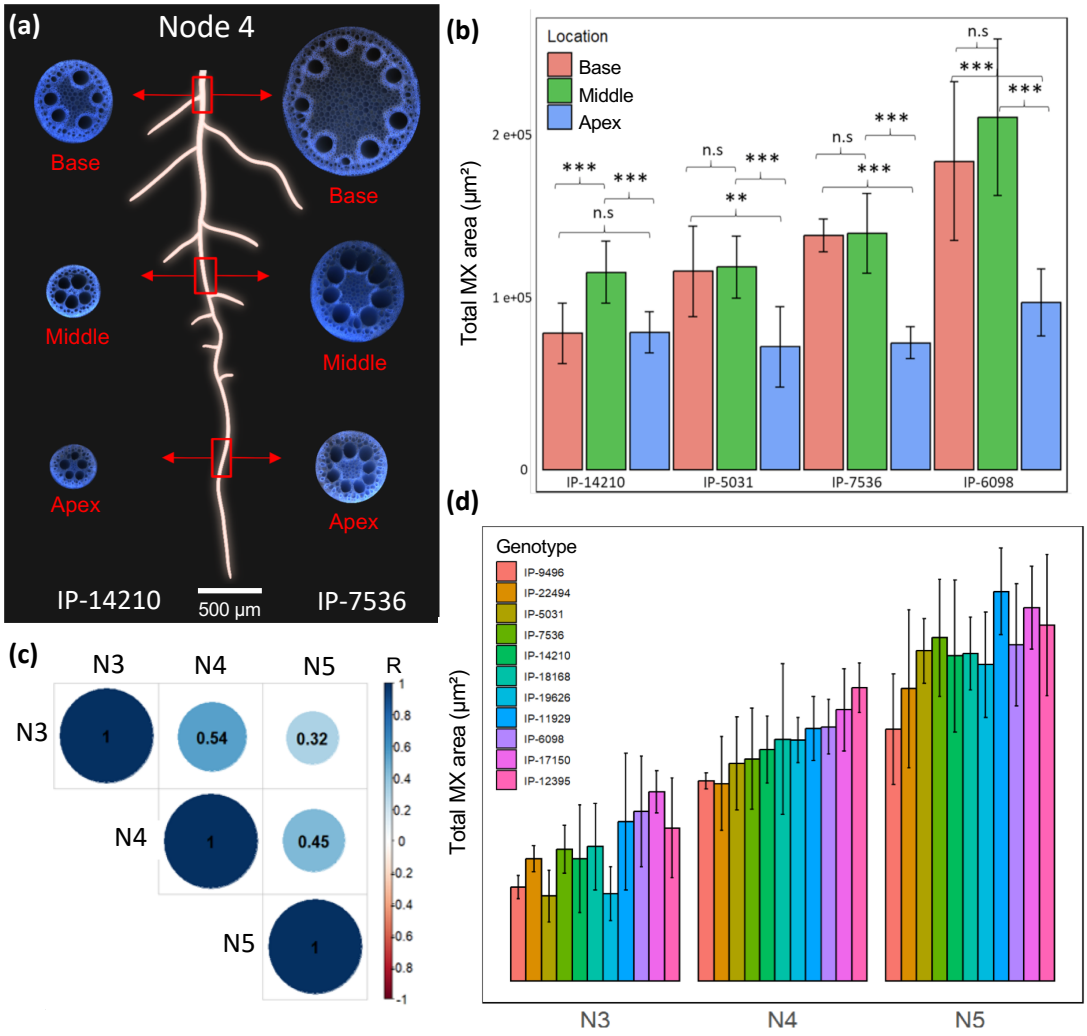

Fig. 3 Total metaxylem area along the crown root from node 4 and in different nodes. (a) Images of root anatomy at three locations (base, middle and apex), along the root length of a crown root sampled from node four in two contrasted genotypes for total metaxylem (MX) area. (b) Total metaxylem area measured at the base, middle and apex of crown roots from node four in four contrasted genotypes for this trait. Plants were grown in rhizotrons under irrigated conditions. ** *p*-value < 0.01, *** *p*-value < 0.001 according to a Student t-test. n.s.: Non-significant. Bars represent means of n = 6 root cross-sectional images per location ± se. (c) Correlation between the total metaxylem area measured at the base of crown roots from node three, four and five. Plants were grown in peat soil under irrigated treatment in the 2023 greenhouse experiment. The Pearson correlation coefficient (R) is indicated for each pair of traits. (d) Genotypes ranking for total metaxylem area measured at the base of crown roots from node three(N3), four (N4) and five (N5). Genotypes were ranked based on their total metaxylem area measured on node four. Plants were grown in the same conditions as in (c). Bars represent means of n = 6 root cross-sectional images per node ± se.

Axial root hydraulic conductance correlates with transpiration restriction under high evaporative demand in dry sandy soil

A positive correlation between total metaxylem area, grain weight and the maintenance of grain weight under vegetative drought stress was observed in the field experiments. As metaxylem vessel size determines axial root conductance, we hypothesised that total metaxylem area could impact transpiration and plant water use under drought stress. To test if total metaxylem area influences transpiration, we monitored the transpiration of genotypes with contrasting total metaxylem areas, grown under irrigated and gradual vegetative drought stress treatments in pots filled with sandy soil in a greenhouse, as evaporative demand increases. At 41 DAS, plant transpiration (Tr) was measured along the day and plant transpiration rate (TR Rate) was plotted against the ETref in order to measure the transpiration response to the evaporative demand, as the slope of the linear regression between these two variables (Slope TR; Fig. **S11**).

The total metaxylem area varied significantly between genotypes (Fig. **S12a**) and significant effect of the drought stress was observed on shoot biomass, indicating that the drought stress was effectively sensed by the plants (Fig. **S12b**). Drought stress did not significantly affect the total metaxylem area and the mean area of individual metaxylem vessels (Fig. **S12c,d**), indicating no drought-induced plastic responses of these traits in this subpanel. Theoretical axial root hydraulic conductance (K_x) was strongly correlated with total metaxylem area (Fig. **S13**) and further used in correlation analyses with plant transpiration as it represents a more physiologically relevant variable. Under irrigated treatment, no correlations were observed between the axial root hydraulic conductance of crown roots from nodes three and four, and the slope of transpiration response to the evaporative demand (Fig. **S14a,b**). Conversely, in the drought stress treatment a negative and significant correlation between the axial root hydraulic conductance of crown roots from node four and the slope of transpiration to the evaporative demand was observed (Fig. **4b**). A similar negative trend, although not significant, was observed with the axial root hydraulic conductance of crown roots from node three (Fig. **4a**). This suggests that under drought stress, plants with larger axial root hydraulic conductance grown in sandy soil restricted their transpiration more when the evaporative demand was the highest, compared to plants with smaller axial root hydraulic conductance.

Higher axial root hydraulic conductance translated into more water use when the water was not limited, as illustrated by the significant positive and significant correlation between the

561 cumulated water use at 41 DAS and the axial root hydraulic conductance of crown roots from
562 node four in the irrigated treatment (Fig. **S15a**). Conversely, when the water was limited,
563 genotypes with higher axial root hydraulic conductance used significantly less water than
564 genotypes with lower axial root hydraulic conductance, as shown by the significant negative
565 correlation between the cumulated water use at 41 DAS and the axial root hydraulic
566 conductance of crown roots from node four in drought stress (Fig. **S15b**). Daily transpiration
567 profiles for two groups of genotypes contrasting for axial root hydraulic conductance but not
568 for shoot biomass (Fig. **S16a**) showed that these responses occur particularly during the hottest
569 hours of the day (Fig. **4c,d**).
570
571 Hence, we conclude that, in sandy soil, plants with larger total metaxylem area and higher axial
572 root hydraulic conductance restrict their transpiration during the hottest hours of the day, thus
573 using less water than plants with smaller total metaxylem area and lower axial root hydraulic
574 conductance. We hypothesise that this mechanism leads to water savings under drought stress.

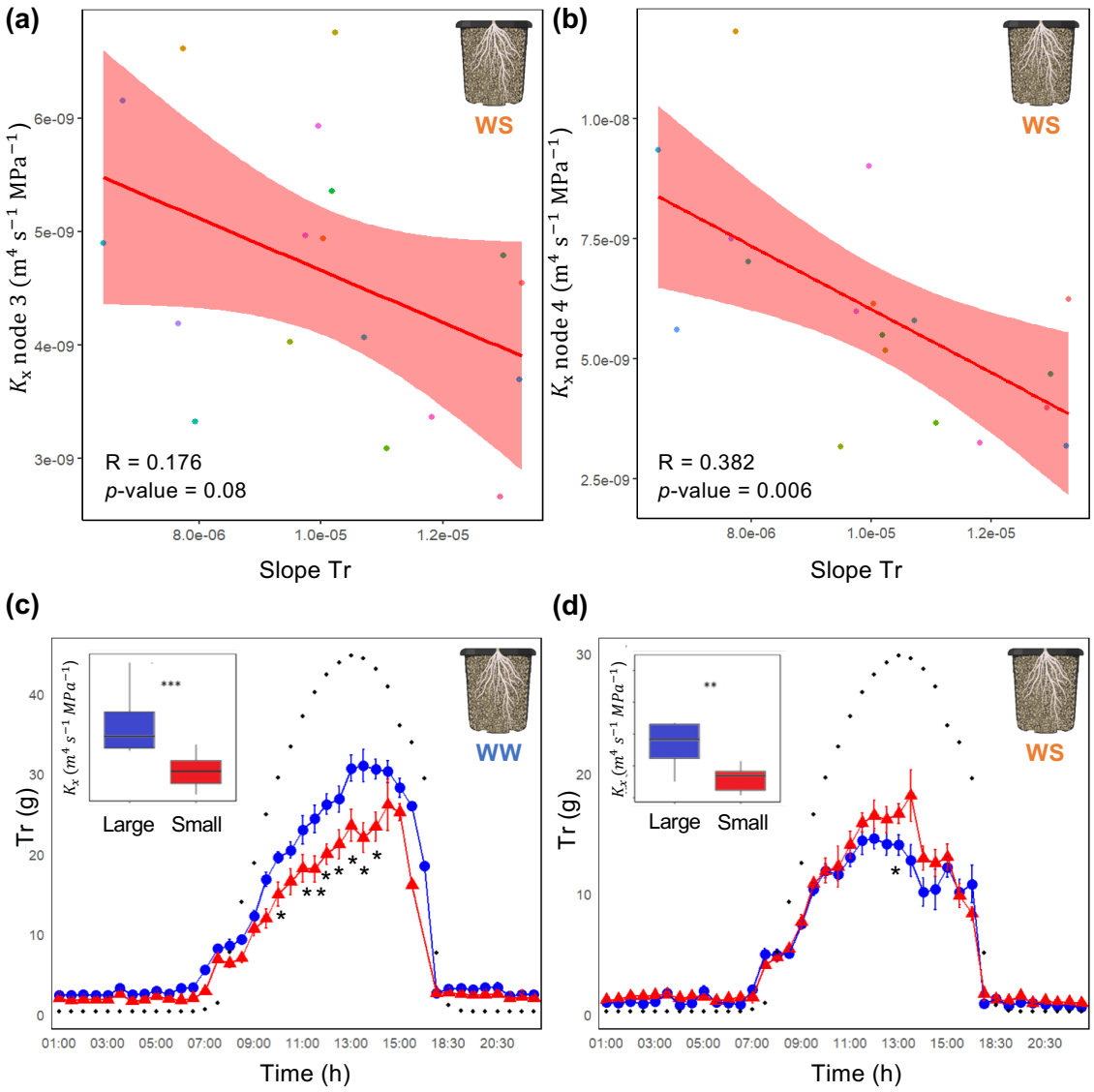

Fig. 4 Association between axial root hydraulic conductance and transpiration response to the evaporative demand in sandy soil. (a, b) Covariation between axial root hydraulic conductance (K_x)measured on crown roots from node three (a) and four (b), and the slope of the transpiration response to the evaporative demand, both measured under drought stress (WS) treatment in the greenhouse. Pearson correlation coefficient (R) and *p*-value of the correlation test are indicated. (c, d) Transpiration (Tr) along the day in two groups of genotypes contrasted for axial root hydraulic conductance (large in blue and small in red)measured under irrigated (c) and drought stress treatments (d). Black dots represent the change in reference evapotranspiration (ETRef) along the day. Significant differences in Tr between the two groups were assessed using a Student t-test. * *p*-value < 0.05.

Soil texture influences the impact of axial root hydraulic conductance on plant transpiration under drought

While our results suggest that larger total metaxylem area are associated with water savings in pearl millet grown under drought in sandy soil, opposite results have been observed in other species (Richards & Passioura, 1989; Salih *et al.*, 1999; Hendel *et al.*, 2021). Recent studies suggest that soil hydraulic properties influence plant transpiration upon soil drying, as well as plant hydraulic traits (Koehler *et al.*, 2023). We therefore tested if the link between total metaxylem area and transpiration restriction at high evaporative demand under drought was conserved in peat soil with different hydraulic properties than sandy soil (higher water retention and hydraulic conductivity as the soil dries; Cai *et al.*, 2022; Wankmüller *et al.*, 2024), using a similar experimental set up in the greenhouse.

In peat soil, the total metaxylem area also varied significantly between genotypes (Fig. **S17a**) and significant effect of the drought stress was observed on shoot biomass but not on the total metaxylem area and the mean area of individual metaxylem vessels (Fig. **S17b, c, d**). A significant positive correlation between the slope of the transpiration response to the evaporative demand and the axial root hydraulic conductance of crown roots from node three was observed in the irrigated treatment, while a similar but non-significant trend was found for crown roots from node four (Fig. **S14c**,**d**). Under drought stress, a significant positive correlation between the slope of transpiration response to the evaporative demand and the axial root hydraulic conductance of crown roots from node three was observed (Fig. **5a**). Although not significant, the same positive trend was observed on crown roots from node four (Fig. **5b**). Transpiration was significantly higher at the hottest hours of the day for genotypes with higher axial root hydraulic conductance in both treatments (Fig. **5c,d**). However, no significant correlations were observed between the cumulated water use and axial root hydraulic conductance when considering all the genotypes in both treatments (Fig **S18a,b**). No significant differences in shoot biomass were observed between these two groups (Fig. **S16b**). This indicates that in the peat soil, plants with larger axial root conductance were more responsive to the evaporative demand under both irrigated and drought stress treatments.

Overall, our results suggest that total metaxylem area and axial root hydraulic conductance influence plant transpiration under drought in a soil-dependent manner. Plants with larger total metaxylem area and axial root hydraulic conductance were able to extract more water from

peat soil than from sandy soil under drought, and the opposite was true for plants with lower total metaxylem area.

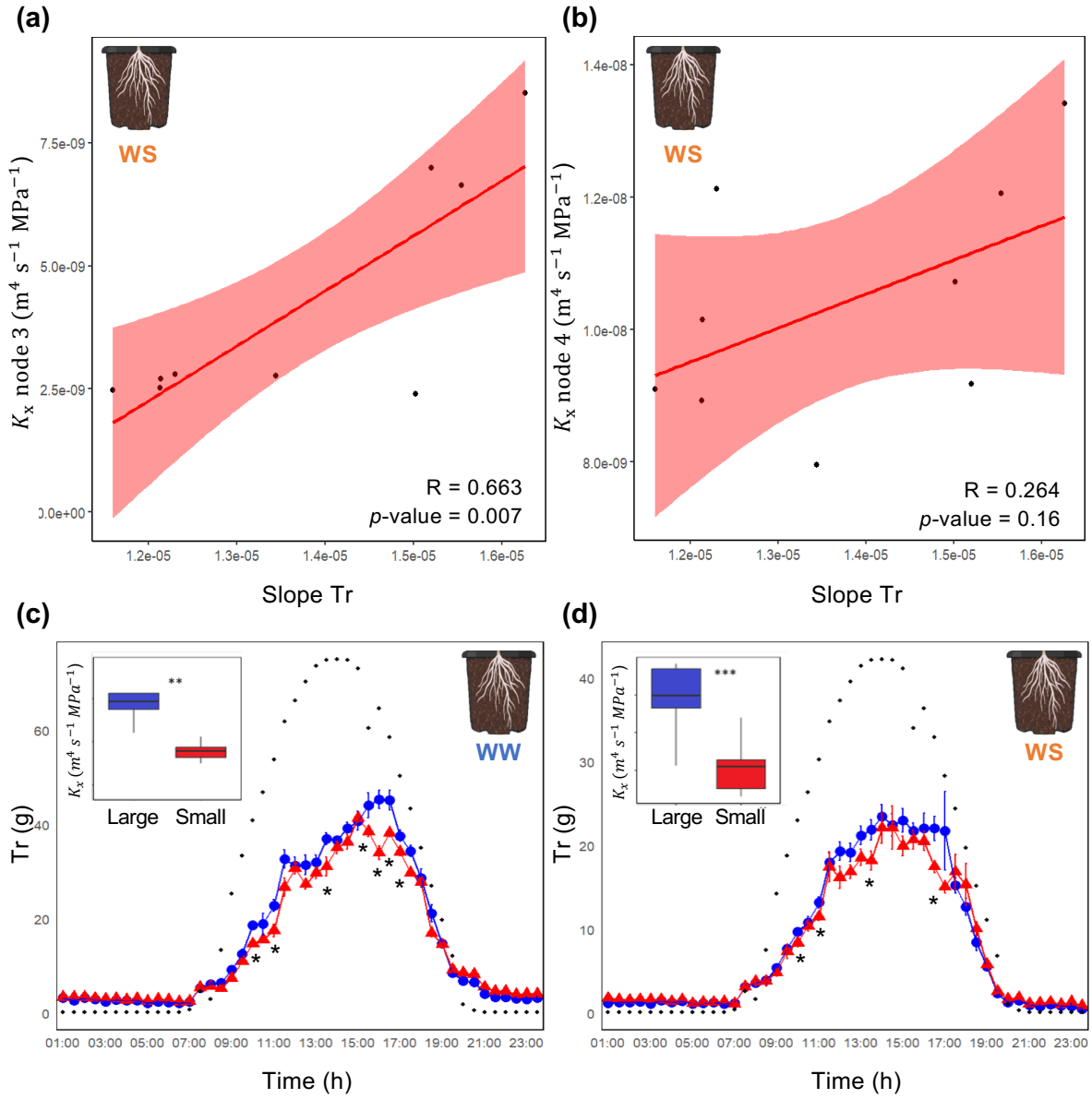

Fig. 5 Association between axial root hydraulic conductance and transpiration response to the evaporative demand in peat soil. (a, b) Covariation between axial root hydraulic conductance (K_x) measured on crown roots from node three (a) and four (b), and the slope of the transpiration response to the evaporative demand, both measured under drought stress (WS) treatment in the greenhouse. Pearson correlation coefficient (R) and *p*-value of the correlation test are indicated. (c, d) Transpiration (Tr) along the day in two groups of genotypes contrasted for axial root hydraulic conductance (large in blue and small in red) measured under irrigated (c) and drought stress treatments (d). Black dots represent the change in reference

evapotranspiration (ETRef) along the day. Significant differences in Tr between the two groups were assessed using a Student t-test. * p-value < 0.05.

Discussion

In this study, we report that traits related to total metaxylem area and mean area of metaxylem were consistently associated with grain weight and its maintenance in pearl millet under vegetative drought stress in the field. Measurements of transpiration dynamics in a greenhouse on a subpanel of genotypes contrasting for total metaxylem area showed that genotypes with larger total metaxylem area on crown roots from nodes three and four (representative of total metaxylem area in roots from subsequent nodes), tended to use more water than genotypes with smaller total metaxylem area under irrigated treatment. Under drought, genotypes with larger total metaxylem area restricted transpiration at the hottest hours of the day and used less water than genotypes with smaller metaxylem vessels in a sandy soil. The transpiration response to evaporative demand observed in sandy soil was reversed in peat soil, which has higher hydraulic conductivity than sandy soil during dry down conditions.

In maize, anatomical phenotyping of roots on node four proved effective in investigating the significance of traits such as cortical cell size and root cortical aerenchyma in drought tolerance (Chimungu *et al.*, 2014b, 2015) or multiseriate cortical aerenchyma in soil compaction (Schneider *et al.*, 2021). In pearl millet, we also phenotyped roots on node four as its development was initiated around the time of drought stress imposition (Ndoye *et al.*, 2024). Our results suggest that total metaxylem area was conserved along the root from the elongation zone to the oldest root base tissue. In line with previous results obtained in maize (Yang *et al.*, 2019), total metaxylem area correlated positively between nodes three to five in eleven pearl millet genotypes contrasting for total metaxylem area, suggesting that anatomical observations of metaxylem-related traits on node four are representative of metaxylem features in subsequent nodes.

Water uptake mainly occurs through crown roots and their laterals in maize (Ahmed *et al.*, 2016, 2018). Similar processes likely occur in pearl millet that does not display seminal roots (Passot *et al.*, 2016) and in which the primary root degenerates a few weeks after germination (ICRISAT, 1981). Water uptake is determined by the speed at which water can be channelled from the soil to the root, i.e. the root hydraulic conductance which can be decomposed into radial and axial conductance. Although radial conductance may represent the most obvious

665 limitation to root hydraulic conductivity, a compelling body of evidence suggest that axial
666 conductance can also be limiting to water uptake in certain plants and environmental conditions
667 (Passioura, 1983; Doussan *et al.*, 1998; Couvreur *et al.*, 2012; Javaux *et al.*, 2013). A limitation
668 comes from the diameter of the vessels which was formalised by Hagen-Poiseuille's law,
669 vessels with lower diameter having lower hydraulic conductance. In maize primary roots,
670 positive correlation was observed between the number and area of metaxylem vessels and the
671 root hydraulic conductivity (Rishmawi *et al.*, 2023). Furthermore, modelling showed that root
672 system conductance was sensitive to axial transport in wheat (Bouda *et al.*, 2018). Considering
673 that metaxylem characteristics were conserved across crown roots, we hypothesised that
674 genotypes with larger metaxylem area on crown root from node four displayed enhanced root
675 hydraulic conductance, with subsequent effects on root water uptake effects and drought
676 tolerance. Although correlations observed between total metaxylem area and drought tolerance
677 measured as grain weight maintenance were significant and robust in the field experiments, the
678 coefficient of correlation was relatively low which may reflect the complexity of different root
679 architectural and anatomical trait interactions on root hydraulics (Maurel & Nacry, 2020).
680 Further architectural phenotyping of genotypes contrasting for total metaxylem area identified
681 in this study should allow better characterization of root hydraulic architecture in pearl millet.
682
683 Plant hydraulics may be modelled as a demand and supply network. Stomatal closure and
684 decreased transpiration will occur when the water supply from the roots becomes insufficient
685 to sustain the demand by the shoot (Vadez *et al.*, 2024). In wet soils, plants with lower root
686 hydraulic conductance would therefore be more rapidly limited in their ability to supply water
687 to the shoots when the evaporative demand increases, which would lead to reduction in
688 transpiration and subsequent water savings (Passioura, 1983). A breeding program in wheat
689 focussed on reducing xylem diameter and the associated axial root hydraulic conductance
690 resulted in deceleration of water use and improved yield in rain-fed environments prone to
691 terminal drought (Richards & Passioura, 1989). Our study also highlights a link between total
692 metaxylem area and water use in pearl millet. Under irrigated treatment, larger total metaxylem
693 area was associated with higher water use as expected. However, larger total metaxylem area
694 was associated with transpiration restriction and decreased water use when the evaporative
695 demand increased under drought stress in sandy soil. To explain this result, we extended the
696 plant supply and demand hydraulic model mentioned above to the soil hydraulics which can
697 have strong impacts on transpiration under drought (Carminati & Javaux, 2020). In maize,
698 comparison of transpiration response to drought stress using hydraulically contrasting soils

showed that transpiration decreased at more negative water potential in loam than in sand (Koehler *et al.*, 2022). This response was linked to an abrupt decrease in soil-root hydraulic conductance at less negative water potential in sand (Koehler *et al.*, 2022). Indeed, sandy soil displays a lower water retention and a steeper decrease in hydraulic conductivity due to their large pores and narrow pore size distribution compared to loam (Cai *et al.*, 2022). It was suggested that while high root hydraulic conductance enables plants to meet high transpiration demand in irrigated soils, it also increases their sensitivity to soil drying in a soil dependent manner (Cai *et al.*, 2022; Wankmüller *et al.*, 2024) - i.e. plants with high root conductance would sense better a decline in soil hydraulic conductivity. Therefore, the relationship between transpiration response to evaporative demand and total metaxylem area that we observed under drought in sandy soil could be linked to the higher sensitivity to decreasing soil conductivity of the more conductive plants.

We propose that, in sandy soils, larger axial root hydraulic conductance due to larger metaxylem area causes a relatively larger drop in leaf water potential relative to the average leaf water potential, leading to a reduction in soil-root conductance triggering stomatal closure and transpiration restriction. We hypothesise that water refilling of the root-soil interface will occur during the night from wet soil not in contact with roots or in contact with roots that are not active. Therefore, the transpiration restriction response would repeat and potentially amplify in subsequent days of soil drying till the fraction of transpirable soil water is null. As the hydraulic properties of the sandy soil used in this study is representative of soil where pearl millet is grown in West Africa, we suggest that similar mechanisms have occurred during the field trials.

Transpiration restriction in response to increased evaporative demand is a mechanism that allows plants to save water at the hottest hours of the day when water loss is poorly rewarded by carbon fixation (Vadez *et al.*, 2023). For this reason, constitutive expression of this phenotype has been linked to increased plant transpiration efficiency (Affortit *et al.*, 2022) or tolerance to terminal drought stress with limited trade-offs (Vadez *et al.*, 2013; Cooper *et al.*, 2014; Sinclair *et al.*, 2017). We propose that the transpiration restriction and subsequent water savings observed in genotypes with larger total metaxylem area under drought in sandy soil contributed to mitigate the impacts of the stress. By saving water, these genotypes would have been better able to maintain their shoot biomass during the drought stress period through improved plant transpiration efficiency. Furthermore, these genotypes were also those better

able to maintain their shoot biomass and grain weight at harvest. Yet, other mechanisms such as plant vigour or flowering time may have contributed to the improved drought tolerance within the panel. A clustering analysis into genotypes with low and high shoot biomass at the end of the drought stress shows that the association between total metaxylem area and grain weight maintenance under drought stress is stronger in the higher shoot biomass cluster which also shows earlier flowering time (Fig. **S19** and **S4**). This suggests that larger total metaxylem area would be particularly beneficial for vegetative drought stress tolerance in vigorous and early flowering genotypes. However, shoot biomass and grain weight measured in the irrigated treatment correlated poorly with these same traits measured in the drought stress treatment (Fig. **S20**), suggesting that vigour was not the main factor explaining drought tolerance. Furthermore, drought stress tended to delay flowering within the panel suggesting no significant drought escapism effects, and no correlation between flowering time and grain weight and its maintenance was observed (Fig. **S4**). These observations support our conclusions that total metaxylem area significantly influenced vegetative drought stress tolerance in pearl millet.

In West Africa, pearl millet landrace variability has already been exploited by farmers to shorten flowering cycles of existing landraces as a response of the 1970s and 1980s drought episodes (Vigouroux *et al.*, 2011; Dussert *et al.*, 2015). Souna3, a popular variety in this region that has been selected for drought tolerance, was included in our field trials. This variety showed average total metaxylem area when compared to the phenotypic diversity observed in the panel, indicating that this trait could still be improved in pearl millet. However, this phenotype may not prove beneficial for all types of drought stress. Plants with larger total metaxylem area will use more water under wet conditions which may enhance the risk of water limitations in case of a terminal drought stress. Further characterization of the genetic determinants controlling metaxylem size should produce genetic materials useful to test these hypotheses in field conditions.

Conclusion

Pearl millet is a cereal crop adapted to arid and semi-arid regions where rain patterns are often erratic and vegetative drought stress can greatly affect grain weight. In sandy soil where pearl millet is typically grown in West Africa, we observed that larger total metaxylem area has benefits for grain weight under irrigated and vegetative drought stress treatments. We propose that larger metaxylem allows increased transpiration when the water is sufficient and water

767 savings through transpiration restriction when water is limited. The hydraulic properties of the
768 sandy soil in which pearl millet is grown may, in relation with plant hydraulics influenced by
769 metaxylem vessel size, be responsible for this shift in water use strategies. Our work reveals
770 the opportunistic nature of pearl millet in terms of water use and highlights how soil hydraulic
771 properties interact with plant hydraulics to influence transpiration along the soil-plant-
772 atmosphere continuum.
773
774 **Acknowledgements**
775 We are grateful to Ghislain Kanfany from ISRA and to Prakash Gangashetty and Mohammed
776 Riyazaddin from ICRISAT for providing seeds of the PMiGAP. We thank the members of the
777 CERAAS and CNRA centres of ISRA for their help during the field experiments in Senegal,
778 and members of the CERES team of the UMR DIADE for their support in the greenhouse
779 experiments in Montpellier. We acknowledge Miranda Niemec for helpful advice on root
780 phenotyping, and Jonathan Lynch, Andrea Carminati and Mathieu Javaux for helpful
781 discussions in the preparation of this manuscript.
782
783 **Funding**
784 This work was supported by the Royal Society (Anatomics grant ICA-R1-180356 to MB and
785 NK), the USAID Feed the Future Sorghum and Millet Innovation lab (GenMil grant
786 n°S19182.01 to NK), the French Institute for Sustainable Development (IRD), the French
787 Ministry for Research and Higher Education (PhD grant to PA) and the Agence National pour
788 la Recherche (PlastiMil grant ANR-17-CE20-0022 to AG).
789
790 **Competing interest**
791 The Authors declare no competing interest.
792
793 **Author contributions**
794 Design of the research: PA, RB, TP, PG, VV, PC, NK, MB, DW, LL, JA, AG; Performance of
795 the research: PA, AF, DJ, EB, BS, JB, MSN, LB, DM, MB, SBK, DW, LL, JA, AG; Data
796 analysis, collection or interpretations: PA, AF, DJ, EB, BS, JB, LB, VV, PC, NK, MB, DW,
797 LL, JA, AG; Writing the manuscript: PA, DJ, MB, DW, LL, JA, AG.
798
799 **Data availability**
800 All datasets are available upon request.

ORCID

Awa Faye https://orcid.org/0000-0001-9222-5976
Dylan H Jones https://orcid.org/0000-0001-8366-1995
Bassirou Sine https://orcid.org/0000-0002-1978-8446
James Burridge https://orcid.org/0000-0002-2194-9894
Mame Sokhatil Ndoye https://orcid.org/0009-0003-8648-6071
Luke Barry https://orcid.org/0009-0004-9652-5246
Stephanie Barnard https://orcid.org/0009-0008-1927-7698
Rahul Bhosale https://orcid.org/0000-0001-6515-4922
Tony Pridmore https://orcid.org/0000-0002-9485-1978
Pascal Gantet https://orcid.org/0000-0003-1314-0187
Vincent Vadez https://orcid.org/0000-0003-2014-0281
Philippe Cubry https://orcid.org/0000-0003-1561-8949
Ndjido Kane https://orcid.org/0000-0002-1879-019X
Malcolm Bennett https://orcid.org/0000-0003-0475-390X
Jonathan A Atkinson https://orcid.org/0000-0003-2815-0812
Laurent Laplaze https://orcid.org/0000-0002-6568-6504
Darren M Wells https://orcid.org/0000-0002-4246-4909
Alexandre Grondin https://orcid.org/0000-0001-6726-6274

References

Affortit P, Effa-Effa B, Ndoye MS, Moukouanga D, Luchaire N, Cabrera-Bosquet L, Perálvarez M, Pilloni R, Welcker C, Champion A, *et al.* 2022. Physiological and genetic control of transpiration efficiency in African rice, *Oryza glaberrima* Steud. *Journal of Experimental Botany* **73**: 5279–5293.

Ahmed MA, Zarebanadkouki M, Kaestner A, Carminati A. 2016. Measurements of water uptake of maize roots: The key function of lateral roots. *Plant and Soil* **398**: 59–77.

Ahmed MA, Zarebanadkouki M, Meunier F, Javaux M, Kaestner A, Carminati A. 2018. Root type matters: Measurement of water uptake by seminal, crown, and lateral roots in maize. *Journal of Experimental Botany* **69**: 1199–1206.

Atkinson JA, Pound MP, Bennett MJ, Wells DM. 2019. Uncovering the hidden half of plants using new advances in root phenotyping. *Current Opinion in Biotechnology* **55**: 1–8.

Bacher H, Montagu A, Herrmann I, Walia H, Schwartz N, Peleg Z. 2023. Stress-induced deeper rooting introgression enhances wheat yield under terminal drought. *Journal of Experimental Botany* **74**: 4862–4874.

Bouda M, Brodersen C, Saiers J. 2018. Whole root system water conductance responds to both axial and radial traits and network topology over natural range of trait variation. *Journal of Theoretical Biology* **456**: 49–61.

Burgarella C, Cubry P, Kane NA, Varshney RK, Mariac C, Liu X, Shi C, Thudi M, Couderc M, Xu X, *et al.* 2018. A western Sahara centre of domestication inferred from pearl millet genomes. *Nature Ecology and Evolution* **2**: 1377–1380.

Burton AL, Williams M, Lynch JP, Brown KM. 2012. RootScan: Software for high-throughput analysis of root anatomical traits. *Plant and Soil* **357**: 189–203.

Cai G, Ahmed MA, Abdalla M, Carminati A. 2022. Root hydraulic phenotypes impacting water uptake in drying soils. *Plant, cell & environment* **45**: 650–663.

Cai G, Ahmed MA, Dippold MA, Zarebanadkouki M, Carminati A. 2020. Linear relation between leaf xylem water potential and transpiration in pearl millet during soil drying. *Plant and Soil* **447**: 579–578.

Cantó-Pastor A, Kajala K, Shaar-Moshe L, Manzano C, Timilsena P, De Bellis D, Gray S, Holbein J, Yang H, Mohammad S, *et al.* 2024. A suberized exodermis is required for tomato drought tolerance. *Nature Plants* **10**: 118–130.

Carminati A, Javaux M. 2020. Soil rather than xylem vulnerability controls stomatal response to drought. *Trends in Plant Science* **25**: 868–880.

Chimungu JG, Brown KM, Lynch JP. 2014a. Reduced root cortical cell file number improves drought tolerance in maize. *Plant Physiology* **166**: 1943–1955.

Chimungu JG, Brown KM, Lynch JP. 2014b. Large root cortical cell size improves drought tolerance in maize (*Zea mays* L.). *Plant Physiology* **166**: 2166–2178.

Chimungu JG, Maliro MFA, Nalivata PC, Kanyama-Phiri G, Brown KM, Lynch JP. 2015. Utility of root cortical aerenchyma under water limited conditions in tropical maize (*Zea mays* L.). *Field Crops Research* **171**: 86–98.

Cooper M, Gho C, Leafgren R, Tang T, Messina C. 2014. Breeding drought-tolerant maize hybrids for the US corn-belt: Discovery to product. *Journal of Experimental Botany* **65**: 6191–6194.

Couvreur V, Vanderborght J, Javaux M. 2012. A simple three-dimensional macroscopic root water uptake model based on the hydraulic architecture approach. *Hydrology and Earth System Sciences* **16**: 2957–2971.

Cunha Neto IL, Hall BT, Lanba AR, Blosenski JD, Onyenedum JG. 2023. Laser ablation tomography (LATscan) as a new tool for anatomical studies of woody plants. *New Phytologist* **239**: 429–444.

Debieu M, Kanfany G, Laplaze L. 2017. Pearl millet genome: Lessons from a tough crop.

Trends in Plant Science **22**: 911–913.
Debieu M, Sine B, Passot S, Grondin A, Akata E, Gangashetty P, Vadez V, Gantet P, Foncéka D, Cournac L, *et al.* 2018. Response to early drought stress and identification of QTLs controlling biomass production under drought in pearl millet. *PLoS ONE* **13**: 1–19.
Diongue DML, Roupsard O, Do FC, Stumpp C, Orange D, Sow S, Jourdan C, Faye S. 2022. Evaluation of parameterisation approaches for estimating soil hydraulic parameters with HYDRUS-1D in the groundnut basin of Senegal. *Hydrological Sciences Journal* **67**: 2327–2343.
Doussan C, Pagès L, Vercambre G. 1998. Modelling of the hydraulic architecture of root systems: An integrated approach to water absorption - Model description. *Annals of Botany* **81**: 213–223.
Dussert Y, Snirc A, Robert T. 2015. Inference of domestication history and differentiation between early- and late-flowering varieties in pearl millet. *Molecular Ecology* **24**: 1387–402.
FAOSTAT. 2024. Food and agricultural data, http://faostat.fao.org/.
Fernandez GC. 1992. Effective selection criteria for assessing plant stress tolerance. In: Kuo C, eds. *Adaptation of food crops to temperature and water stress*. Shanhua, Taiwan: The World Vegetable Center, 257–270.
Fuente C, Diouf MN, Ndour PMS, Debieu M, Grondin A, Passot S, Champion A, Barrachina C, Pratlong M, Gantet P, *et al.* 2022. Genetic control of rhizosheath formation in pearl millet. *Scientific Reports* **12**: 1–13.
Fuente C, Grondin A, Sine B, Debieu M, Belin C, Hajjarpoor A, Atkinson JA, Passot S, Salson M, Orjuela J, *et al.* 2024. Glutaredoxin regulation of primary root growth confers early drought stress tolerance in pearl millet. *eLife*. doi: https://doi.org/10.7554/eLife.86169.3
Hall B, Lanba A, Lynch JP. 2019. Three-dimensional analysis of biological systems via a novel laser ablation technique. *Journal of Laser Applications*. doi: https///doi.org/10.2351/1.5096089
Hendel E, Bacher H, Oksenberg A, Walia H, Schwartz N, Peleg Z. 2021. Deciphering the genetic basis of wheat seminal root anatomy uncovers ancestral axial conductance alleles. *Plant Cell and Environment* **44**: 1921–1934.
Henry A, Cal AJ, Batoto TC, Torres RO, Serraj R. 2012. Root attributes affecting water uptake of rice (*Oryza sativa*) under drought. *Journal of Experimental Botany* **63**: 4751–4763.
ICRISAT. Maiti R, Bidinger F. 1981. Bulletin no. 6, *Growth and development of the pearl millet plant*. Patancheru, India: ICRISAT Press.
Javaux M, Couvreur V, Vanderborght J, Vereecken H. 2013. Root water uptake: From three-dimensional biophysical processes to macroscopic modeling approaches. *Vadose Zone Journal* **12**: 1–16.
Kar S, Tanaka R, Korbu LB, Kholová J, Iwata H, Durbha SS, Adinarayana J, Vadez V. 2020. Automated discretization of 'transpiration restriction to increasing VPD' features from outdoors high-throughput phenotyping data. *Plant Methods* **16**: 1–20.
Koehler T, Moser DS, Botezatu Á, Murugesan T, Kaliamoorthy S, Zarebanadkouki M, Bienert MD, Bienert GP, Carminati A, Kholová J, *et al.* 2022. Going underground: Soil hydraulic properties impacting maize responsiveness to water deficit. *Plant and Soil*. **478**: 43–58.
Koehler T, Schaum C, Tung SY, Steiner F, Tyborski N, Wild AJ, Akale A, Pausch J, Lueders T, Wolfrum S, *et al.* 2023. Above and belowground traits impacting transpiration decline during soil drying in 48 maize (*Zea mays*) genotypes. *Annals of Botany* **131**: 373–386.
Li A, Zhu L, Xu W, Liu L, Teng G. 2022. Recent advances in methods for in situ root phenotyping. *PeerJ* **10**: 1–29.
Lynch JP, Chimungu JG, Brown KM. 2014. Root anatomical phenes associated with water

acquisition from drying soil: targets for crop improvement. *Journal of Experimental Botany* **65**: 6155–6166.

Lynch JP, Mooney SJ, Strock CF, Schneider HM. **2021**. Future roots for future soils. *Plant Cell and Environment* **45**: 620–636.

Mahalakshmi V, Bidinger F, Raju D. **1987**. Effect of timing of water deficit on pearl millet (*Pennisetum americanum*). *Field Crops Research* **15**: 327–339.

Maurel C, Nacry P. **2020**. Root architecture and hydraulics converge for acclimation to changing water availability. *Nature Plants* **6**: 744–749.

Millet EJ, Rodriguez Alvarez MX, Perez Valencia DM, Sanchez I, Hilgert N, van Rossum B-J. **2021**. StatgenHTP: High throughout phenotyping (HTP) data analysis. *R package version 1.0.5*: https://CRAN.R-project.org/package=statgenHTP.

Ndoye MS, Burridge J, Bhosale R, Grondin A, Laplaze L. **2022**. Root traits for low input agroecosystems in Africa : Lessons from three case studies. *Plant, Cell and Environment* **45**: 637–649.

Ndoye MS, Lucas M, Ajmera IB, Sine B, Faye A, Burridge J, Ngom M, Gantet P, Wells DM, Kane NA, *et al.* 2024. Modeling reveals synergies among root traits for phosphorus acquisition in pearl millet. *Crop Design*. doi: https://doi.org/10.1016/j.cropd.2024.100059

Nobel PS. **2009**. *Physicochemical and Environmental Plant Physiology. 4th edition*. Cambridge, UK: Academic Press.

Passioura JB. **1983**. Roots and drought resistance. *Agricultural Water Management* **7**: 265–280.

Passot S, Gnacko F, Moukouanga D, Lucas M, Guyomarc'h S, Ortega BM, Atkinson JA, Belko MN, Bennett MJ, Gantet P, *et al.* 2016. Characterization of pearl millet root architecture and anatomy reveals three types of lateral roots. *Frontiers in plant science*. doi: https://doi.org/10.3389/fpls.2016.00829

Pound MP, French AP, Wells DM, Bennett MJ, Pridmorea TP. **2012**. CellSeT: Novel software to extract and analyze structured networks of plant cells from confocal images. *Plant Cell* **24**: 1353–1361.

Richards RA, Passioura JB. **1989**. A breeding program to reduce the diameter of the major xylem vessel in the seminal roots of wheat and its effect on grain yield in rain-fed environments. *Australian Journal of Agricultural Research* **40**: 943–950.

Rishmawi L, Bauget F, Protto V, Bauland C, Nacry P, Maurel C. **2023**. Natural variation of maize root hydraulic architecture underlies highly diverse water uptake capacities. *Plant Physiology* **192**: 2404–2418.

Rodríguez-Álvarez MX, Boer MP, van Eeuwijk FA, Eilers PHC. **2018**. Correcting for spatial heterogeneity in plant breeding experiments with P-splines. *Spatial Statistics* **23**: 52–71.

van Rossum B. **2024**. statgenGxE: Genotype by Environment (GxE) Analysis. : R package version 1.0.9. URL https://github.com/Biometrics/statgenGxE/

Salih AA, Ali IA, Lux A, Luxova M, Cohen Y, Sugimoto Y, Inanaga S. **1999**. Rooting, water uptake, and xylem structure adaptation to drought of two sorghum cultivars. *Crop Science* **39**: 168–173.

Salson M, Orjuela J, Mariac C, Zekraouï L, Couderc M, Arribat S, Rodde N, Faye A, Kane NA, Tranchant-Dubreuil C, *et al.* 2023. An improved assembly of the pearl millet reference genome using Oxford Nanopore long reads and optical mapping. *G3: Genes, Genomes, Genetics* **13**: 1–7.

Schneider HM, Strock CF, Hanlon MT, Vanhees DJ, Perkins AC, Ajmera IB, Sidhu JS, Mooney SJ, Brown KM, Lynch JP. **2021**. Multiseriate cortical sclerenchyma enhance root penetration in compacted soils. *Proceedings of the National Academy of Sciences*. doi: https://doi.org/10.1073/pnas.2012087118

Sehgal D, Skot L, Singh R, Srivastava RK, Das SP, Taunk J, Sharma PC, Pal R, Raj B, Hash CT, *et al.* 2015. Exploring potential of pearl millet germplasm association panel for association mapping of drought tolerance traits. *PLoS ONE* **10**: 1–28.

Sidhu JS, Lynch JP. **2024**. Cortical cell size regulates root metabolic cost. *Plant Journal* **118**: 1343–1357.

Sinclair TR, Devi J, Shekoofa A, Choudhary S, Sadok W, Vadez V, Riar M, Rufty T. **2017**. Limited-transpiration response to high vapor pressure deficit in crop species. *Plant Science* **260**: 109–118.

Strock CF, Schneider HM, Galindo-Castañeda T, Hall BT, Van Gansbeke B, Mather DE, Roth MG, Chilvers MI, Guo X, Brown K, *et al.* 2019. Laser ablation tomography for visualization of root colonization by edaphic organisms. *Journal of Experimental Botany* **70**: 5327–5342.

Sultan B, Gaetani M. **2016**. Agriculture in west africa in the twenty-first century: Climate change and impacts scenarios, and potential for adaptation. *Frontiers in Plant Science* **7**: 1–20.

Trachsel S, Kaeppler SM, Brown KM, Lynch JP. **2011**. Shovelomics: High throughput phenotyping of maize (*Zea mays* L.) root architecture in the field. *Plant and Soil* **341**: 75–87.

Uga Y, Sugimoto K, Ogawa S, Rane J, Ishitani M, Hara N, Kitomi Y, Inukai Y, Ono K, Kanno N, *et al.* 2013. Control of root system architecture by DEEPER ROOTING 1 increases rice yield under drought conditions. *Nature genetics* **45**: 1097–102.

Vadez V, Grondin A, Chenu K, Henry A, Laplaze L, Millet EJ, Carminati A. **2024**. Crop traits and production under drought. *Nature reviews earth & environment*. doi: https://doi.org/10.1038/s43017-023-00514-w

Vadez V, Kholová J, Yadav RS, Hash CT. **2013**. Small temporal differences in water uptake among varieties of pearl millet (*Pennisetum glaucum* (L.) R. Br.) are critical for grain yield under terminal drought. *Plant and Soil* **371**: 447–462.

Vadez V, Pilloni R, Grondin A, Hajjarpoor A, Belhouchette H, Brouziyne Y, Chehbouni G, Kharrou MH, Zitouna-Chebbi R, Mekki I, *et al.* 2023. Water use efficiency across scales: From genes to landscapes. *Journal of Experimental Botany* **16**: 4770–4788.

Varshney RK, Shi C, Thudi M, Mariac C, Wallace J, Qi P, Zhang H, Zhao Y, Wang X, Rathore A, *et al.* 2017. Pearl millet genome sequence provides a resource to improve agronomic traits in arid environments. *Nature Biotechnology* **35**: 969–976.

Vigouroux Y, Mariac C, de Mita S, Pham JL, Gérard B, Kapran I, Sagnard F, Deu M, Chantereau J, Ali A, *et al.* 2011. Selection for earlier flowering crop associated with climatic variations in the Sahel. *PLoS ONE* **6**: 1–9.

Wankmüller FJP, Delval L, Lehmann P, Baur MJ, Cecere A, Wolf S, Or D, Javaux M, Carminati A. **2024**. Global influence of soil texture on ecosystem water limitation. *Nature*. doi: https://doi.org/10.1038/s41586-024-08089-2

Winkel T, Renno JF, Payne WA. **1997**. Effect of the timing of water deficit on growth, phenology and yield of pearl millet (*Pennisetum glaucum* (L.) R. Br.) grown in Sahelian conditions. *Journal of Experimental Botany* **48**: 1001–1009.

Yang JT, Schneider HM, Brown KM, Lynch JP. **2019**. Genotypic variation and nitrogen stress effects on root anatomy in maize are node specific. *Journal of Experimental Botany* **70**: 5311–5325.

Zhu J, Brown KM, Lynch JP. **2010**. Root cortical aerenchyma improves the drought tolerance of maize (*Zea mays* L.). *Plant, Cell and Environment* **33**: 740–749.

Zotarelli L, Dukes MD, Romero CC, Migliaccio KW, Morgan KT. **2010**. Step by Step Calculation of the Penman-Monteith Evapotranspiration (FAO-56 Method). *University of Florida Institute Department of Agricultural and Biological Engineering*. doi: https://doi.org/10.32473/edis-ae459-2010

Supporting Information

Table S1 Weather data collected during the field trials in 2021 and 2022.

Supplementary file S1 Passport data of the different pearl millet lines used in this study.

Fig. S1 Field trials experimental design.

Fig. S2 Volumetric soil water content in the 2021 and 2022 field trials at two depth intervals (0-60 cm and 60-120 cm) measured using DIVINER probes.

Fig. S3 An example cross-sectional image of a crown root from node four obtained through laser ablation tomography and tissue annotation using the pearl millet version of RootScan.

Fig. S4 Correlation between shoot morphological and agronomical traits measured in the field across both years (2021 and 2022) in the irrigated (WW) and drought stress (WS) treatments.

Fig. S5 Stress impact on plant height, tiller number and 1000-grain weight measured in the field across both treatments (WW: Irrigated; WS: Drought stress) and years (2021 and 2022).

Fig. S6 Covariation between stress tolerance index for shoot biomass measured in both years (2021 and 2022).

Fig. S7 Correlation between root anatomical traits measured in the field across both years (2021 and 2022) in the irrigated (WW) and drought stress (WS) treatments.

Fig. S8 Stress impact on total metaxylem vessel area, mean area of metaxylem, number of metaxylem, root cross section area, stele area, ratio of stele area to root cross section area (SR ratio), sclerenchyma area and ratio of sclerenchyma to root cross section area (SCL ratio).

Fig. S9 Correlation between root anatomical traits, grain weight (GW), and stress tolerance index for grain weight (STI GW) measured under irrigated treatment in the 2021 and 2022 field experiments.

Fig. S10 Correlation between the number of metaxylem vessels along the crown root of node four and across different nodes.

Fig. S11 Transpiration response to the evaporative demand in pearl millet genotypes grown in the greenhouse under irrigated (WW) and drought stress (WS) treatments.

Fig. S12 Stress impact on shoot biomass and metaxylem-related traits in pearl millet genotypes contrasting for total metaxylem area.

Fig. S13 Covariation between total area of metaxylem and axial root hydraulic conductance.

Fig. S14 Covariation between axial root hydraulic conductance (K_x) measured in crown roots from node three and four, and the transpiration response to the evaporative demand (Slope Tr) in pearl millet genotypes contrasting for total metaxylem area grown under irrigated treatment in the greenhouse.

1055 **Fig. S15** Water use in pearl millet genotypes contrasting for total metaxylem area grown under
1056 irrigated (WW) and drought stress (WS) treatments in sandy soil in the greenhouse.
1057 **Fig. S16** Shoot biomass in two groups of genotypes contrasting for axial root hydraulic
1058 conductance (K_x; large versus small) measured under the drought stress treatment.
1059 **Fig. S17** Stress impact on shoot biomass and metaxylem-related traits in pearl millet genotypes
1060 contrasting for total metaxylem area. Plants were grown in the greenhouse in peat soil.
1061 **Fig. S18** Water use in pearl millet genotypes contrasting for total metaxylem area grown under
1062 irrigated (WW) and drought stress (WS) treatments in peat soil in the greenhouse.
1063 **Fig. S19** Covariation between total metaxylem area and stress tolerance index for grain weight.
1064 **Fig. S20** Covariation of shoot biomass and grain yield between both treatments within years.